Seasonality of Water Column Methane Oxidation and Deoxygenation in a Dynamic Marine Environment

Qianhui Qin[a], Franklin S. Kinnaman[b], Kelsey M. Gosselin[a], Na Liu[a], Tina Treude[c,d], and David L. Valentine[b,*]

[a]Interdepartmental Graduate Program in Marine Science, University of California, Santa Barbara, CA 93106, USA

[b]Department of Earth Science and Marine Science Institute, University of California, Santa Barbara, CA 93106, USA

[c]Department of Earth, Planetary and Space Sciences, University of California, Los Angeles, Los Angeles, CA 90095, USA

[d]Department of Atmospheric and Oceanic Sciences, University of California, Los Angeles, Los Angeles, CA 90095, USA

Abstract

Most of the methane input to the world's oceans is intercepted by microorganisms in sediment and the overlying water column and oxidized before it has an opportunity to reach the atmosphere, where it acts as a greenhouse gas. The factors controlling methane consumption in the ocean are not well established and its biogeochemistry in dynamic marine environments is understudied in-part because of challenges in capturing spatial and temporal variability. Our study focused on the factors that structure methane's biogeochemistry in a dynamic marine environment, the Santa Barbara Basin. The deep-water column of the Santa Barbara Basin experiences seasonal oxygen loss and episodic replenishment which we found to be major factors in structuring the

accumulation of methane and the rate at which microorganisms consumed that methane. We found the gradual decline in oxygen that commonly occurs through the summer culminated with a pronounced accumulation of methane in the water column during the fall. Rates of methane oxidation remained low in summer, increased with the buildup of methane in fall, and remained elevated into spring, even after methane concentration had declined. However, results from methane oxidation kinetics experiments revealed a zero-order kinetic dependence on oxygen concentration, indicating that oxygen's effect on methanotrophy at the ecosystem scale is likely indirect. We also captured an apparent mixing event during fall that drove spatial and temporal variability in oxygen, nitrate and methane concentrations in the Santa Barbara Basin, with stark variations at the investigated timescale of 8 days and along isobaths at a spatial scale of 7 km. Collectively, these results indicate the seasonal development and attenuation of a methanotrophic community associated with restricted circulation, but also of a spatiotemporal variability not previously appreciated for this environment.

Keywords: aerobic methanotrophy; dissolved methane; dissolved oxygen; nitrate; seasonal hypoxia; dynamic marine environment

1. Introduction

The ocean is not a major source of methane to the atmosphere (~ 4-15 Tg yr^{-1}, less than 2.5% of total methane sources, Solomon et al., 2007), even though a significant amount of methane (at least 85 Tg yr^{-1}) is consistently produced in marine environments through microbial or thermal transformation of organic carbon (Hinrichs et al., 1999; Reeburgh, 2007; Zhang et al., 2011; Reay et al., 2018). Instead, anaerobic oxidation of methane (AOM) occurs in marine sediment, and

together with aerobic methane oxidation (hereafter MOx) near to the seafloor and in the overlying water column, acts as a biological filter (Reeburgh, 2007; Mau et al., 2013; Torres-Beltrán et al., 2016; Steinle et al., 2017). AOM can consume ~75% - 80% of the produced methane in the sediment (Strous and Jetten, 2004; Treude, 2004; Knittel and Boetius, 2009; Torres-Beltrán et al., 2016) and commonly occurs at a banded interface in the sediment known as the sulfate-methane transition zone. In diffusive systems, AOM usually quantitatively consumes sedimentary methane (Knittel and Boetius, 2009), but in sediments with advective transport or gas ebullition methane can bypass the benthic microbial filter and enter the water column (Reeburgh, 2007; Knittel and Boetius, 2009).

Since the first measurements of dissolved methane concentrations in the ocean's water column were reported in the late 1960s (Reeburgh, 2007), various groups have studied water column methane concentrations and MOx rates in different oceanic environments (Griffiths et al., 1982; Ward et al., 1987, 1989; Reeburgh et al., 1991; de Angelis et al., 1993; Ward and Kilpatrick, 1993; Valentine et al., 2001; Mau et al., 2012, 2013; Heintz et al., 2012; Pack et al., 2015; Steinle et al., 2015, 2016, 2017). Most studies represent snapshots of oceanographic conditions and have collectively demonstrated that the rate of MOx depends on the availability and concentrations of the two substrates of the reaction, methane and oxygen, together with other physicochemical controls like temperature, salinity, nutrients, etc (Ward et al., 1987; Valentine et al., 2001; Mau et al., 2012, 2013; Heintz et al., 2012; Pack et al., 2015; Steinle et al., 2015, 2016).

Many oceanic environments are dynamic because of seasonal, spatial, and other physiochemical factors. Methane concentration and MOx rate variability together control the atmospheric release

of methane and knowledge of these processes is therefore import for predicting future changes in methane emissions. Numerous studies have considered the spatial variability of MOx (Reeburgh, 2007; Mau et al., 2012, 2013; Steinle et al., 2016), but fewer studies have considered the temporal variability (Tavormina et al., 2010; Kessler et al., 2011; Heintz et al., 2012; Crespo-Medina et al., 2014; Steinle et al., 2015, 2017; Torres-Beltrán et al., 2016) and the coupled understanding of spatial and temporal variability for MOx is minimal (Gründger et al., 2021).

The Santa Barbara Basin (SBB) is a depression between the California mainland and the northern Channel Islands. The SBB is physically constrained and experiences seasonal deoxygenation. The maximum water depth is about 589 m at the depocenter and the deep basin is fully enclosed at depths >475m. The SBB is bounded by a shallow Eastern sill, and exchanges water with the Pacific Ocean over the 475m Western sill. Because of the depth difference between sill and depocenter, SBB bottom waters are poorly circulated and are regularly deoxygenated (to <1 μM O_2) following periods of increased surface productivity (Bograd et al., 2002; Goericke et al., 2015). Low oxygen condition is interrupted ~annually by strong springtime upwelling events where deep-water cascades over the sill from the greater Pacific and into the SBB. In the process, existing bottom waters are flushed and the deep SBB becomes temporarily oxygenated to ~20 μM. The introduced oxygen gets quickly consumed by heterotrophic organisms scavenging organic matter, and the deep water oxygen concentration returns to <1 μM, typically by the end of summer (Sholkovitz and Gieskes, 1971; Sholkovitz, 1973; Sholkovitz and Soutar, 1975; Reimers et al., 1990; Goericke et al., 2015). SBB bottom water is low in oxygen throughout the year, and is classified as hypoxic seawater (oxygen concentration <63 μM, according to Middelburg and Levin, 2009). As reference, seawater at a temperature of 5 ºC and a salinity of 34 PSU, which is typical for SBB deep water,

would have an oxygen concentration of ~319 μM when in equilibrium with the atmospheric gases at 1 atm pressure (Weiss, 1970).

A temporal perspective for the SBB derives from the long-term hydrographic data set collected by the California Cooperative Oceanic Fisheries Investigations (CalCOFI), since 1986 (https://calcofi.org/data/). A compilation of relevant CalCOFI data (Fig 1) illustrates the seasonal deoxygenation pattern of the SBB deep water column. Bottom water dissolved oxygen and nitrate typically peak in spring with upwelling events, and then gradually decrease after, until the next upwelling events occur. The seasonal deoxygenation occurs ~annually, typically coupled with extensive denitrification (Sigman et al., 2003).

The SBB is known for having one of the largest natural methane seep areas in the world, thus many previous studies focused on this environment (Hornafius et al., 1999; Hill et al., 2003; Mau et al., 2007, 2010; Ding and Valentine, 2008; Du et al., 2014; Padilla et al., 2019; Joung et al., 2020). The deeper water column of the SBB has been less studied with regard to methane due to the logistical challenges that arise with monitoring methane-related processes over time. In the deep SBB the methane sources are mainly diagenetic (Warford et al., 1979; Kosiur and Warford, 1979; Li et al., 2009) with methane produced by benthic methanogenic archaea and consumed mainly anaerobically by archaea in the sediment and by aerobic bacteria in the water column (Hinrichs et al., 2003; Pack et al., 2011). This study aims to build on our understanding of methane dynamics in low oxygen marine systems. Our goal is to construct a depth-resolved time series of methane concentration and oxidation rate nested within the seasonal cycle of oxygen decline and renewal in the deep SBB. Furthermore, we also aim to explore the factors influencing kinetics of methane

oxidation. In doing so, this study identified unanticipated spatiotemporal variability of key compounds – methane, oxygen and nitrate – within the enclosed reaches of the SBB.

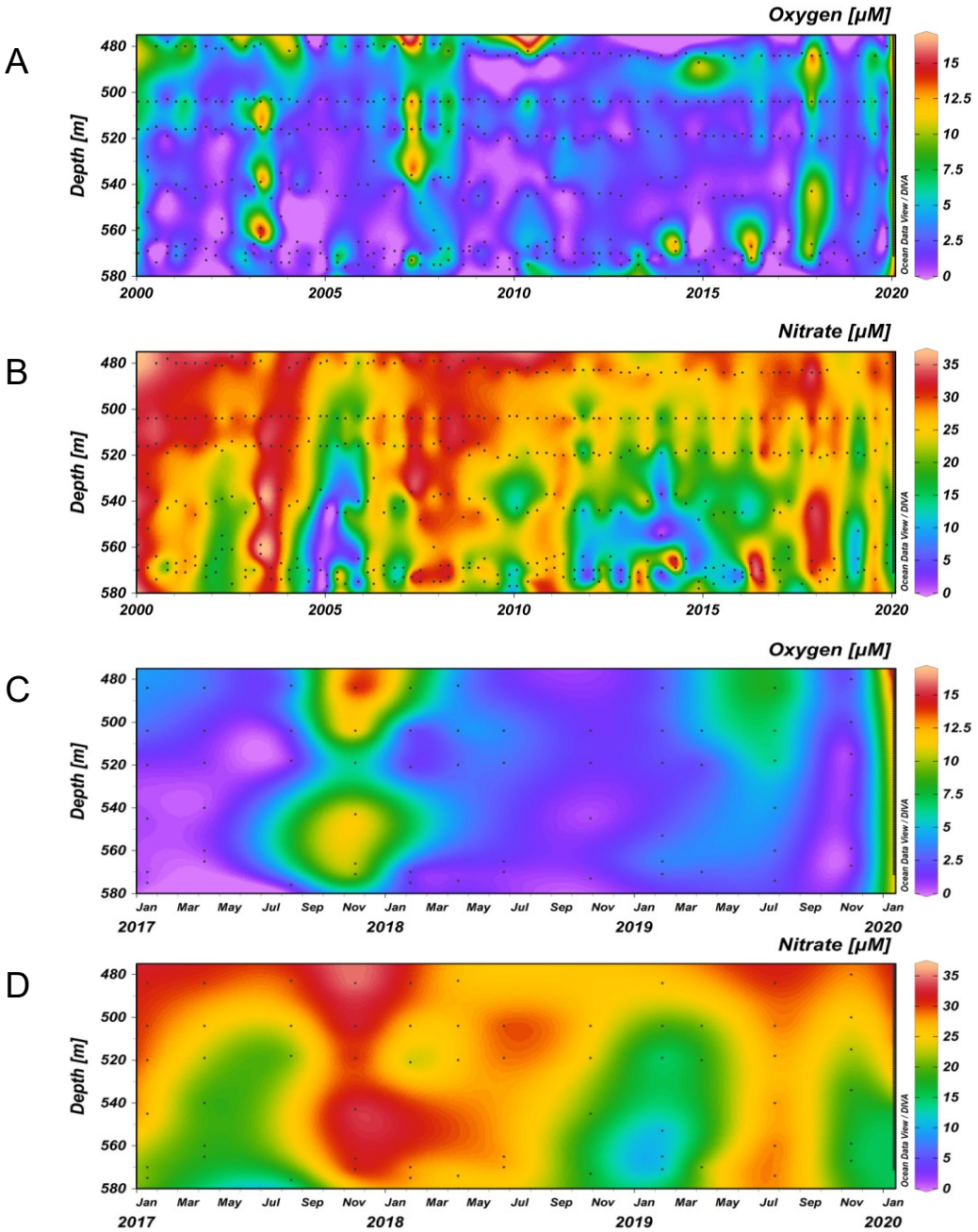

Figure 1. SBB deep water column (475m-580m) heat maps from 2000-2020 of A) oxygen concentration and B) nitrate concentration, as well as higher resolution heat maps from 2017-2020 of C) oxygen concentration and D) nitrate concentration. Black dots represent the original data points, all data are from CalCOFI.

2. Materials and Methods

2.1 Sampling Time and Locations

Our sampling plan involved the collection of deep-water column samples from the SBB throughout a deoxygenation and reoxygenation cycle, with a sampling time span of ~one year. Within this year, one to two sampling expeditions were executed every month. Restrictions associated with the COVID-19 pandemic prevented any sampling from the end of March 2020, limiting the time span of our study to 266 days. Nonetheless, we were still able to capture key features of the cycle as presented in this work. Sampling was conducted from several different research vessels (Table 1), with the first sampling expedition executed on 2019-6-28, 15 more sampling expeditions (18 more hydrocasts) performed afterwards, with the last sampling expedition conducted on 2020-3-20.

A series of 10 sampling expeditions using UCSB's *R/V Connell* were conducted to collect deep SBB water samples, in order to study the changes of deep SBB water column oxygen, nitrate, and methane concentrations, and MOx rates. During each *R/V Connell* sampling, a rosette equipped with 6 4-liter Niskin bottles was deployed and deep-water samples of six different depths were collected (Table 1). These six depths were selected to emphasize changes in deep water characteristics, especially for depths lower than the western sill (depth > 475m). The in-situ temperature profiles were recorded by a conductivity–temperature–depth (CTD) package (Seabird SBE 19+ V2 SeaCAT Profiler) attached to the rosette.

Five additional hydrocasts were conducted during the AT42-19 BASIN19 cruise (2019-10-29 to 2019-11-10) onboard *R/V Atlantis*, using *R/V Atlantis*' CTD (Seabird 911+) rosette with 24 10-

liter Niskin bottles. In-situ temperature was recorded by CTD, in-situ oxygen concentration was recorded by an oxygen sensor that was mounted on the rosette. Water samples were collected for four of these five hydrocasts, from 24 depths. And for the collected water samples, oxygen concentrations were measured using ODF Winkler titration method, nitrate concentrations were measured by flow injection analysis, methane concentrations were measured using a headspace equilibration method.

Available data from four additional cruises were also used for time series analysis including: water column oxygen concentrations from cruise SR1919 onboard *R/V Sally Ride*, which took place in December 2019 (data provided by Dr. Alyson Santoro); oxygen and nitrate concentration data collected by CalCOFI during three quarterly surveys CalCOFI 1907BH, CalCOFI 1911OC, and CalCOFI 2001RL (Data available on CalCOFI's website).

All samples were collected from three different stations within the deep SBB: CalCOFI station 081.8 046.9 (CalCOFI here after), which lies to the north of the shipping lanes that cut across SBB, with a position of (34.2749, -120.0252); South Depocenter Radius Origin (SDRO), which lies to the south of the shipping lanes, with the position (34.2008, -120.0417); and North Depocenter Radius Origin (NDRO), which also lies to the north of the shipping lane, with the position (34.2625, -120.0313). The distance between station NDRO and SDRO is ~7 km. Stations were selected arbitrarily within the depocenter of the SBB, and were treated interchangeably (based on an assumption of lateral homogeneity) when external factors (strong winds, fog, rough seas, shipping traffic) favored access to one station over another. The sampling depths and additional details about samples and measurements are listed in Table 1.

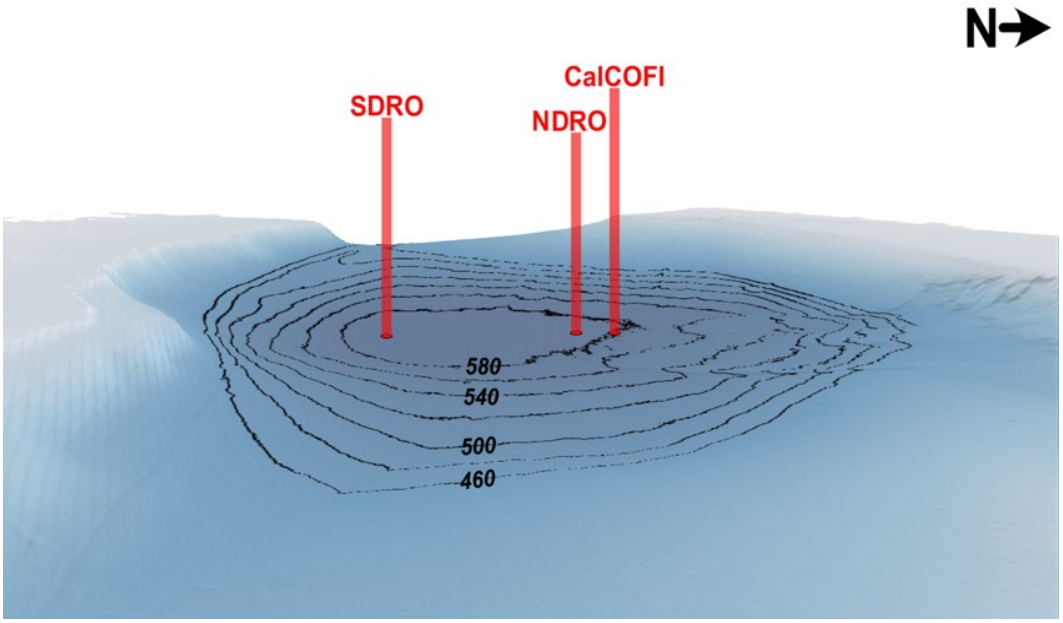

Figure 2. Bathymetry of the deep Santa Barbara Basin including the three sampling stations: SDRO, NDRO, CalCOFI – occupied in this study. The coordinates of the stations are: Station SDRO, 34.2008 N, 120.0497 W; Station NDRO, 34.2681 N, 120.0433 W; Station CALCOFI, 34.2749 N, 120.0252 W.

Table 1. Data and samples used for this study.

Sampling Date	Season	Cruise Number	Station	Sampling Depths (m)	Analyses Performed
2019-06-28	Summer	Connell-062819	CalCOFI	50, 300, 440, 500, 540, 570	a, c, e, f
2019-07-18	Summer	Connell-071819	SDRO	450, 500, 520, 540, 560, 580	a, c, e, f
2019-07-26	Summer	CalCOFI 1907BH	CalCOFI	444, 484, 504, 518, 540, 560, 574	a, c
2019-08-01	Summer	Connell-080119	CalCOFI	450, 500, 520, 540, 560, 570	a, c, e, f
2019-08-13*	Summer	Connell-081319	SDRO	450, 500, 520, 540, 560, 580	a, c, e,
2019-08-26*	Summer	Connell-082619	SDRO	450, 500, 520, 540, 560, 580	a, c, e,
2019-09-24	Fall	Connell-092419	CalCOFI	450, 500, 520, 540, 560, 570	a, c, e, f
2019-10-04	Fall	Connell-100419	CalCOFI	450, 500, 520, 540, 560, 570	a, c, e, f
2019-10-21	Fall	Connell-102119	SDRO	450, 500, 520, 540, 560, 580	a, c, e, f
2019-10-30	Fall	AT42-19 BASIN19	NDRO	b: 1m resolved from 450-577 e: 450, 465, 475, 490, 500-575 (every 5 m), 577	b, e
2019-10-30	Fall	AT42-19 BASIN19	SDRO	a and c: 450, 475, 490, 500, 510-580 (every 5 m), 583 b: 1m resolved from 450-583 e: 450, 475, 515-580 (every 5 m), 583	a, b, c, e
2019-11-03	Fall	AT42-19 BASIN19	NDRO	b: 1m resolved from 450-574	b

2019-11-07	Fall	AT42-19 BASIN19	NDRO	b: 1m resolved from 450-576 c and e: 450, 465, 475, 490, 500-575 (every 5 m), 576	b, c, e
2019-11-07	Fall	AT42-19 BASIN19	SDRO	a: 450, 500, 520, 540, 560, 580 b: 1m resolved from 450-580 c: 450, 475, 490, 500, 510-580 (every 5m), 581 e: 450, 475, 490, 500, 520-580 (every 5m), 581	a, b, c, e
2019-11-15	Fall	CalCOFI 1911OC	CalCOFI	440, 480, 500, 515, 534, 559, 567	a, c
2019-12-19	Winter	SR1919	CalCOFI	b: 1m resolved from 450-572	b
2020-01-16	Winter	CalCOFI 2001RL	CalCOFI	1m resolved from 450-571	b, d
2020-02-06[#]	Winter	Connell-020620	CalCOFI	500, 560, 570	a, c, e, f
2020-03-19	Spring	Connell-031920	CalCOFI	450, 500, 520, 540, 560, 570	a, c, e, f

The abbreviations stand for the following types of analyses performed:
a = oxygen concentration measured by the Winkler titration method;
b = oxygen concentration measured by the CTD attached oxygen sensor;
c = nitrate concentration;
d = nitrate concentration measured by the CTD attached nitrate sensor;
e = methane concentration;
f = fractional methane turnover rate.
[*]: Fractional methane turnover rate data of 2019-8-13 and 2019-8-26 were discarded because of sampling apparatus problem.
[#]: For 2020-2-6, all data of 450, 520 and 540 m were discarded because of sampling apparatus malfunction.

2.2 Dissolved Oxygen Concentration Sample Collection and Measurement

Dissolved oxygen concentration sample collection and measurement were conducted using a University of California, San Diego Oceanographic Data Facility (ODF) designed automated titration system. Deep water samples were collected by Niskin bottles and introduced into Winkler flasks through Tygon tubing immediately after the Niskin bottles were opened. Per depth, two replicate samples were collected. Each Winkler flask was filled for at least 3 volumes of water to overflow. Temperature was recorded for each sample during the overflow process. After the water sample was collected, manganese chloride and sodium hydroxide-sodium iodide were added below surface of liquid into the flask immediately, then a ground glass stopper was inserted, and

the flask was inverted several times to mix the reagents with the seawater. After precipitates formed (~30 min), the flasks were inverted several times again to make sure the reagents acted fully. Then the samples were transported to lab with water around the neck of the flask to prevent air from entering the flask during transportation, and then stored in the dark until analysis.

Back in the lab, dissolved oxygen concentration was measured by ODF automated titration system. Sulfuric acid was added just before analyzing to free iodine, and then oxygen concentration was measured by an automated oxygen titrator using photometric end-point detection based on the absorption of 365 nm wavelength ultra-violet light.

2.3 Nitrate Concentration Sample Collection and Analysis

Dissolved nitrate concentration sample collection was conducted following UCSB Marine Science Institute Analytical Lab's requirement. Deep water samples from Niskin bottles were filtered through a 0.4 μm polycarbonate filter introduced into clean, pre-rinsed plastic HDPE 20 mL scintillation vials. ~17 mL water was filtered into each vial, and then the vial was capped closed. Per depth, two replicate samples were collected. Dissolved nitrate concentrations were analyzed in the deep-water samples by flow injection analysis (FIA) according to the procedure described by (Segarra Guerrero et al., 1996) using the QuikChem 8500 Series 2 (Lachat Instruments, Zellweger Analytics Inc.).

2.4 Dissolved Methane Concentration Sample Collection and Analysis

Dissolved methane concentration sample collection and analysis were made as described in Heintz et al., 2012, with the following modifications: Seawater was collected by Niskin bottles and

introduced into 120 mL serum bottles using 20-30 cm length Tygon tubing with long glass tips. The serum bottles were filled from bottom to the top and flushed 3 times of their volume to minimize contact of the sampled water with the surrounding air. The serum bottles were then closed carefully without gas bubbles using chlorobutyl stoppers and then crimp sealed. For each depth, duplicate methane concentration samples were collected immediately after oxygen concentration samples. The samples were kept cold during transport back to lab for analysis. Samples were preserved using 0.3 mL of 10M NaOH solution by volume exchange with water. For the *R/V Connell* cruises, samples were preserved upon return to the laboratory, 2-4 hours following collection. For the BASIN19 cruise, samples were preserved shipboard ~ 1 hour after collection. Following addition of the preservative, 10 mL headspace of ultrahigh-purity nitrogen (Airgas Ultra High Purity Grade Nitrogen, Manufacturer Part #:UHP300) was added by displacement into each bottle. Then the sample bottles with headspace were shaken vigorously for 1 minute and left upside down in the dark at 4°C for one day to equilibrate. After equilibration, an aliquot of 2 mL of the headspace was taken out using a syringe and injected to either a Shimadzu GC-14A or Shimadzu GC-8A equipped with flame ionization detector to measure the methane concentration in the headspace. For GC-14A, a 100 μL sample loop and a 3.66 m, 2-mm inner-diameter, n-octane Res-Sil C packed column (Restek) with N_2 as the carrier gas (20 mL min^{-1} flow rate) were used (Kinnaman et al., 2007). For GC-8A, the same setting was used except that the sample loop was 500 μL. Calibration standards were obtained from Scott Specialty Gasses and Gasco Precision Calibration Mixtures, and a minimum three-point calibration was conducted daily prior to analyzing samples. Analyses were performed both shipboard (for BASIN19 cruise) and upon return to the laboratory (for *R/V Connell* cruises) with the same instrument and standards. All samples were analyzed within 2 weeks.

243

244 **2.5 Fractional Methane Turnover Rate Sample Collection and Analysis**

245 The fractional methane turnover rate (d^{-1}) is defined as the ratio of the activity of ^3H in the produced
246 water divided by the total activity of ^3H in the sample, then further divided by the incubation time
247 of the sample (days) shown in Eq. 1.

248 $$Fractional\ methane\ turnover\ rate = \frac{^3H-H_2O}{^3H-CH_4+^3H-H_2O} * \frac{1}{incubation\ time} \quad \text{(Eq. 1)}$$

249 Sample collection was similar to methane concentrations (see above), except that seawater was
250 introduced to 72 mL serum bottles. Three replicate samples were collected per depth.

251

252 The fractional methane turnover rate was analyzed based on the ^3H-labeled methane incubation
253 protocol by Bussmann et al., 2015, with the following modifications: In the lab, approximately 10
254 µL of gaseous ^3H-CH_4 tracer (~0.8 kBq, specific activity 37-740 GBq·mmol^{-1}) was added into
255 each sample bottle and the bottle was shaken vigorously for 2 min to facilitate dissolution of
256 methane. Then the samples were kept in the dark at in-situ temperature (5-7°C) and incubated for
257 68-90 hours. After incubation with ^3H-CH_4 for approximately three days, samples were taken out
258 from the incubator and microbial activity was stopped by adding 0.2 mL 25% H_2SO_4. Then the
259 sample bottles were opened, and immediately a 2 mL aliquot was pipetted each into two 7 mL
260 scintillation vials. To one of the 7 mL scintillation vials immediately 5 mL scintillation cocktail
261 (Ultima Gold LLT) was added followed by liquid scintillation counting (Beckman LS 6500) to
262 determine ^3H-CH_4 + ^3H-H_2O. The aliquot in the other 7 mL scintillation vial was air-bubbled for
263 5 minutes to remove ^3H-CH_4 before adding scintillation cocktail and liquid scintillation counting
264 to determine ^3H-H_2O.

265

266 For all sampling expeditions involving methane turnover rate determinations, three additional
267 bottles were prepared the same way as the samples, from three out of the six sampling depths, one
268 sample of each depth, to serve as killed controls. For controls, 0.2 mL 25% H_2SO_4 was added first
269 to stop the microbial activity before the addition of ^3H-CH_4. For the majority of the samples, the
270 resulting activities in killed controls were several orders of magnitude lower compared to samples.
271 A mathematical test to determine the level of detection was also performed on the methane
272 turnover rate results. Samples whose methane turnover rate values were higher than the average
273 killed control value plus three times of the standard deviation were kept. For the samples with
274 methane turnover rate values lower than the level of detection (21 out of 126 samples), their
275 methane turnover rates were considered zero. For samples with values higher than the level of
276 detection, mean values of controls were subtracted from sample values in order to correct for minor
277 amounts of impurity in the stock solution and any abiotic conversion.
278

279 **2.6 MOx Rate Calculation**

280 Microbially mediated MOx occurs ideally by the reaction shown in Eq. 2.

281 $$CH_4 + 2O_2 \rightarrow CO_2 + 2H_2O \quad \text{(Eq. 2)}$$

282 We used fractional methane turnover rate and ambient methane concentration to calculate the
283 methane oxidation rate, assuming adherence to the first-order rate law (Eq. 3), and assuming the
284 oxidation rate is proportional to methane concentration (Valentine et al., 2001).

285 $$r_{ox} = k' \times [CH_4] \quad \text{(Eq. 3)}$$

286 r_{ox} is the methane oxidation rate (concentration per time), and k' is the effective first-order rate
287 constant (time^{-1}). In our experiment setting, k' has the value of the measured fractional methane

turnover rate, and [CH_4] is the ambient methane concentration. All methane oxidation rates were calculated according to Eq. 3.

Since we only added a very small amount of ^3H-CH_4 into each sample bottle, the ambient methane concentration was increased insignificantly (~0.01-0.04 nM). Therefore, ambient methane concentrations were used for the calculation of MOx.

2.7 Time Course Experiment to Validate Incubation Duration

Incubation time for methane turnover rate measurement was 3 days according to Bussmann et al., 2015. To verify this, a time course experiment was also performed on samples from Connell-092419 to test if the uptake rate of ^3H-CH_4 is linear over the incubation time. Nine samples were collected at each sampling depth (6 sampling depths in total), and then divided into 3 groups of triplicate samples. Each sample was treated the same, with ~10 μL ^3H-CH_4 tracer and then incubated in the dark at in-situ temperature for 1, 2, and 2.85 days in group 1, 2, 3, respectively. At the end of the incubation, samples were killed and oxidation rates quantified as described above.

2.8 Oxygen or Methane Concentration as a Control on MOx Rate

Oxygen and methane concentration alteration experiments were performed to test the influence of oxygen and methane concentration on MOx rate. The purpose of the two experiments was to test the assumption that MOx in the SBB deep water column follows assumed kinetic behavior. The oxygen concentration alteration experiment was conducted on samples from Connell-100419 (Table 1). Nine samples were collected at each sampling depth, and then divided into 3 groups of triplicate samples. Group 1 had ambient oxygen concentrations (the average value of two measured

311 replicate samples). Group 2 was treated with an addition of 30 μL pure oxygen using a 100 μL
312 gas-tight syringe (SGE, 23G, bevel type tip), which increased the oxygen concentration by 17.6
313 μM. Group 3 was treated with an addition of 60 μL pure oxygen, which increased the oxygen
314 concentration by 35.2 μM. The methane concentration alteration experiment was conducted on
315 samples from Connell-092419 (Table 1). Nine samples were collected at each sampling depth, and
316 then divided into 3 groups of triplicate samples. Group 1 had ambient methane concentrations (the
317 average value of two measured replicate samples). Group 2 was treated with an addition of 4 μL
318 4% gaseous methane (96% N_2) using a 25 μL gas-tight syringe (SGE, 23G, bevel type tip), which
319 increased the methane concentration by 100 nM. Group 3 was treated with an addition of 12 μL
320 4% gaseous methane (96% N_2), which increased the methane concentration by 300 nM. For both
321 concentration alteration experiments, 10 μL ^3H-CH_4 tracer was added into each sample bottle after
322 altering initial oxygen or methane of the sample bottle, and incubated at in-situ temperature in the
323 dark for 3 days. Fractional methane turnover rates were measured from each incubation, and MOx
324 rate was calculated based on first order kinetics assumption. The resulting MOx rates were plotted
325 against initial oxygen or methane concentrations to evaluate the influences of oxygen or methane
326 concentrations on MOx.
327

328 Table 2. Sample and treatment information of the experiments to test controls of MOx rate by
329 oxygen and methane concentrations.

Depth (m)	Group 1/Ambient		Group 2	Group 3
	Average $[O_2]$ (μM)	Percentage difference (%)	$[O_2]$ (μM)	$[O_2]$ (μM)
450	11.9	10.0	29.5	47.1
500	10.4	1.0	28.0	45.6
520	4.6	7.4	22.2	39.8
540	3.6	12.3	21.2	38.8
560	4.2	NA	21.8	39.4
570	4.8	10.0	22.5	40.1

	Average $[CH_4]$ (nM)	Percentage difference (%)	$[CH_4]$ (nM)	$[CH_4]$ (nM)
450	15	1.7	115	315
500	55	1.5	155	355
520	87	7.6	187	387
540	82	7.2	182	382
560	133	6.0	233	433
580	220	12.7	320	520

Control of MOx rate by oxygen concentration, samples are from Connell-100419.
Control of MOx rate by methane concentration, samples are from Connell-102119.

2.9 Visualization of Time Series Data

Time series maps were generated using Ocean Data View version 5.6.0-64 bit. For each sampling date and each sampling depth, the average value of duplicate (oxygen, nitrate and methane concentrations) or triplicate (MOx rate) samples was used. Gridded fields were calculated using DIVA gridding algorithm, with X scale-length of 400 and Y scale-length of 350. We chose a slightly higher value for X scale-length to highlight the changes with time.

2.10 Depth-Integrated Oxygen and Methane Concentrations

Depth-integrated oxygen and methane concentrations were estimated by calculating the area under the oxygen and methane concentration depth profile curves of 2019-10-30 and 2019-11-07 to demonstrate the spatiotemporal variability of oxygen and methane for this 8-day interval.

3. Results

3.1 Time Series of Water Column Parameters

To describe time-course changes of solute concentrations and MOx rates, we divided the deep SBB water column (440m to bottom) into three layers based on biogeochemical patterns: top layer, 440 – 500 m; middle layer, 500 – 550 m; and bottom layer, 550 m – seafloor. We further divided

time by season to capture temporal changes of the measured parameters: summer (June, July and August); fall (September, October and November); winter (December, January and February); spring (March, April and May).

Oxygen concentrations started at an average of ~12 μM in the deep SBB water column in early summer 2019, with the lowest concentration in the middle layer (Fig 3A). Oxygen concentration subsequently decreased throughout the SBB deep water column, with the bottom layer experiencing the most rapid decline. By early fall 2019, the bottom and middle layers, and the lower part of the upper layer all exhibited oxygen concentration <5 μM. The only exception was the upper reaches of the top layer, which had an oxygen concentration of ~10 μM. During this three-month period (June to September), dissolved oxygen decreased by ~12 μM for the bottom layer, ~4 μM for the middle layer, and ~2 μM for the top layer. Low oxygen conditions persisted for fall 2019, with a gradual subsequent increase apparent from winter 2019.

Nitrate concentration displayed a similar vertical pattern as oxygen concentration in early summer 2019, with the lowest concentration in the middle layer ~25 μM, and higher concentrations in the top and bottom layers, ~30 μM (Fig 3B). Nitrate concentration decreased throughout fall 2019, reaching an observed minimum of ~19 μM in the bottom layer in mid fall 2019. Starting from January 2020 (mid winter), nitrate concentration gradually increased with time.

For the five sampling events in summer 2019 (Connell-062819, Connell-071819, Connell-080119, Connell-081319, and Connell-082619), methane concentrations were relatively low throughout the deep water column (Fig 3C). Even at the deepest sampling depth, methane concentrations were

less than 25 nM. Starting from early fall 2019, we observed a substantial increase of methane concentration in the bottom layer. A trend of exponential increase persisted for about a month and expanded from the bottom to the middle layer. Conversely, the top layer experienced minimal change. Methane concentration reached its peak value at late fall, to ~300 nM, followed by a rapid decline. From late October to early November, methane concentration decreased by more than half in the middle and bottom layer. By early spring 2020, deep water methane concentration returned to <25 nM in the bottom layer.

For the three sampling events in summer 2019 (Connell-062819, Connell-071819, and Connell-080119), MOx rates (Fig 3D) were low throughout the water column. For the top and middle layers, MOx rates were less than 0.05 $nM \cdot d^{-1}$; for the bottom layer, MOx rates were slightly higher, ~0.2 $nM \cdot d^{-1}$. Starting from early fall 2019, MOx rates began to increase. The increase was first observed in the bottom layer, where MOx rates increased to ~0.5 $nM \cdot d^{-1}$ on Connell-092419 (early fall), followed by an increased MOx rate in the middle layer. On Connell-100419 (mid fall), bottom layer MOx rates reached a peak value of 2.5 $nM \cdot d^{-1}$. The increase of MOx rates was concurrent with the increase of methane concentration in the deep water column, indicative of an active microbial response. On Connell-102119 (mid fall 2019), MOx rates for the bottom and middle layers remained high; rates declined for the two sampling events in late winter and early spring 2020, though more gradually compared to the abrupt decrease in methane concentration. For the final sampling event on Connell-031920 (early spring 2020), MOx rates were still relatively high compared to the initial sampling events, despite similarly low methane concentration.

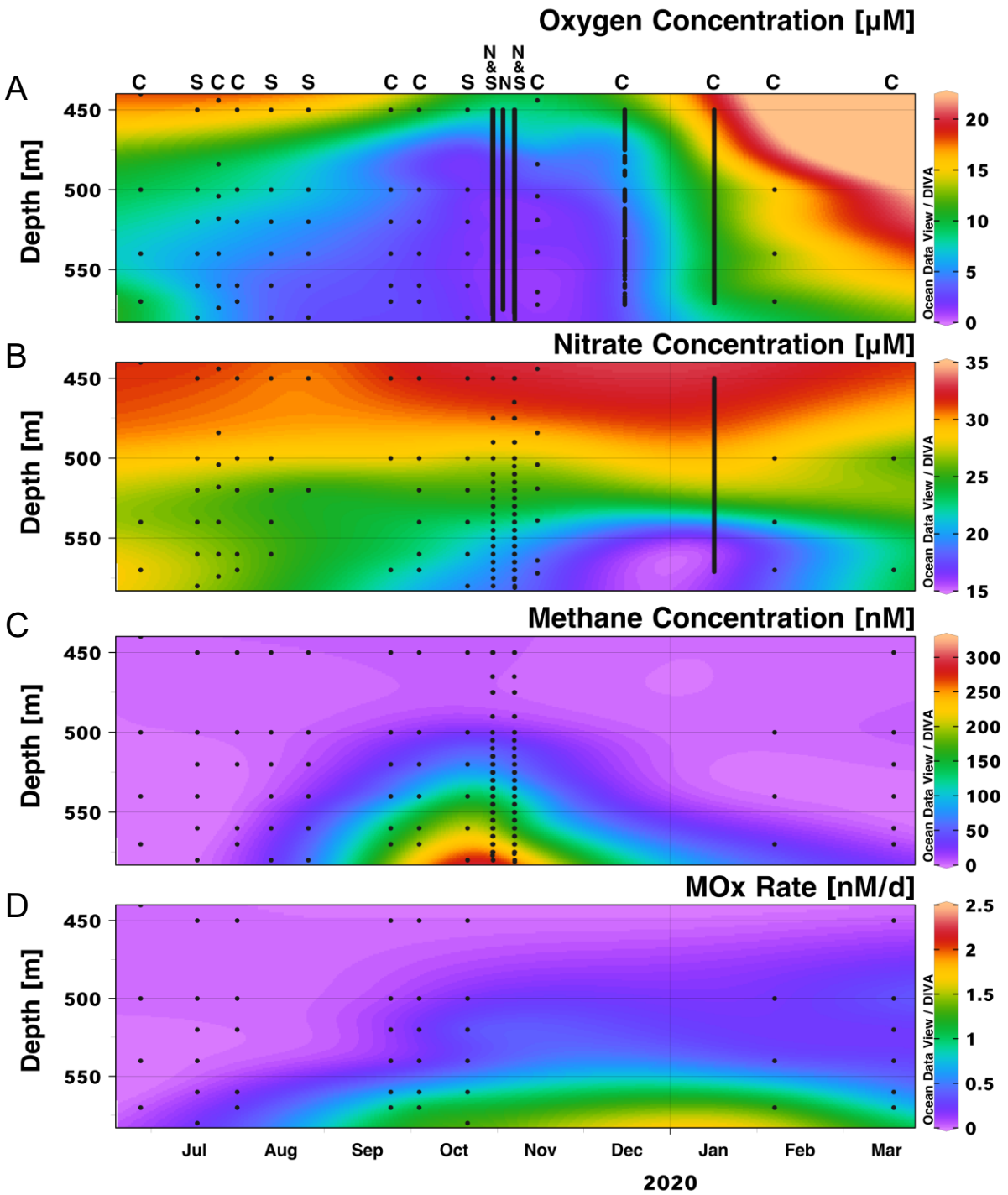

Figure 3. Interpolated time series of (from A to D) oxygen concentration, nitrate concentration, methane concentration and MOx rate of the deep SBB water column (440m-583m) from 2019-6-28 to 2020-3-19. Data are from samples of three sampling stations: SDRO, NDRO, CalCOFI. These three stations within the deep SBB were treated in aggregate and are identified as follows: S=SDRO; N=NDRO; and C= CalCOFI. Black dots denote average value of duplicate (for

oxygen, nitrate and methane concentrations) or triplicate (for MOx rate) samples from each depth.

3.2 Variability at Short Spatial and Temporal Scales

Time series data collected for this study originated from three stations in the Deep Santa Barbara Basin, which we initially considered to be interchangeable based on the assumption of lateral homogeneity. To test this assumption, we compared the oxygen and methane concentration profiles at two stations (NDRO and SDRO, with a distance of 7 km) sampled in rapid succession on 2019-10-30 and again on 2019-11-07. From the four resulting depth profiles (Fig 4A, 4B, 4D and 4E) we identify substantial spatial and temporal variability.

On 2019-10-30, the oxygen content of the SBB deep water was similar between SDRO and NDRO, with a consistent decrease from 450 m to 500 m depth and a uniform concentration below 500 m, as is apparent in their difference plot (Fig 4G). The depth-integrated amount of oxygen was similar for the two stations, 246 $mmol \cdot m^{-2}$ for NDRO and 274 $mmol \cdot m^{-2}$ for SDRO. Methane exhibited somewhat greater variability on this date. While both stations contained similar integrated quantities of methane (17.1 $mmol \cdot m^{-2}$ for NDRO and 17.2 $mmol \cdot m^{-2}$ for SDRO), that methane was distributed to shallower depths at NDRO.

In contrast to the consistency observed between stations on 2019-10-30, substantial heterogeneity was apparent on 2019-11-7. At NDRO, there was an increased amount (~220 $mmol \cdot m^{-2}$, from 246 $mmol \cdot m^{-2}$ on 2019-10-30 to 466 $mmol \cdot m^{-2}$ on 2019-11-7) of oxygen in the top layer of the deep SBB, whereas SDRO exhibited substantially increased oxygen (~137 $mmol \cdot m^{-2}$, from 274 $mmol \cdot m^{-2}$ on 2019-10-30 to 411 $mmol \cdot m^{-2}$ on 2019-11-7) together in both the top layer and the

middle layer. Both stations experienced significant drops in methane concentration throughout the middle and bottom layers of the deep water column. The depth-integrated quantity of methane, dropped by ~11.5 mmol·m^{-2} (67% of the amount on 2019-10-30) for NDRO, and dropped by ~14.5 mmol·m^{-2} (84% of the amount on 2019-10-30) for SDRO. Station SDRO exhibited a greater methane concentration decline compared to station NDRO. On 2019-11-7, station SDRO exhibited less integrated oxygen (~55 mmol·m^{-2}) and methane (~2.8 mmol·m^{-2}) throughout the deep water column compared to station NDRO, as shown by Fig 4H.

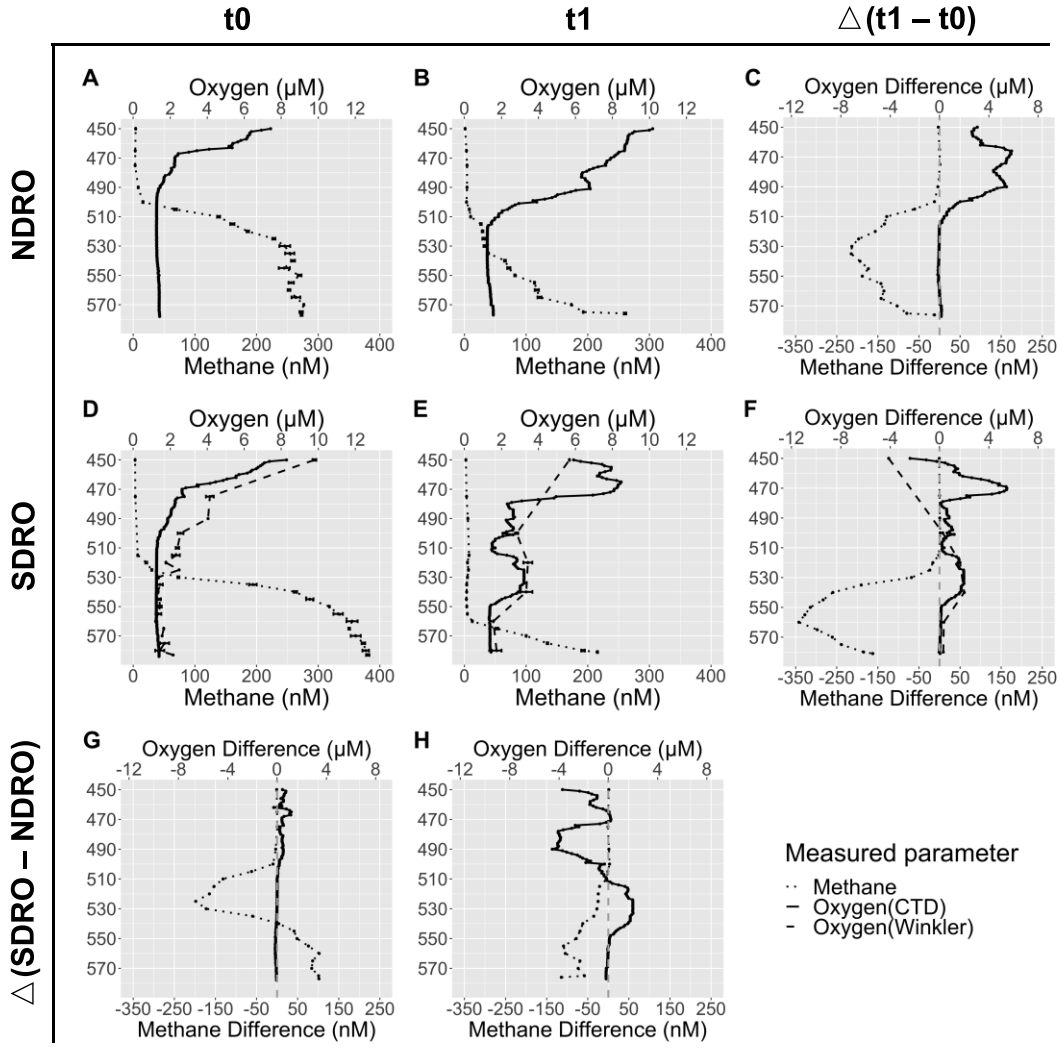

Figure 4. Depth profiles showing the variability of oxygen and methane in the deep water column of the SBB at short spatial and time scales. t0 denotes 2019-10-30, t1 denotes 2019-11-7.

t1-t0 describes the difference between 8 days. Dotted lines are measured methane concentration values; Solid lines are oxygen concentration values determined by a CTD-mounted oxygen sensor, while dashed lines are oxygen concentration values determined by Winkler titration. Gray dashed vertical lines in G and H indicate no difference. All the y-axes are depths ranging from 450 m to 584 m. A) Depth profiles of NDRO on 2019-10-30; B) Depth profiles of NDRO on 2019-11-7; C) Time difference profiles of NDRO, positive values indicate concentration increase over time, negative values indicate concentration decrease over time; D) Depth profiles of SDRO on 2019-10-30; E) Depth profiles of SDRO on 2019-11-7; F) Time difference profiles of SDRO; G) Station difference profiles of 2019-10-30, positive values indicate higher concentrations at SDRO, negative values indicate higher concentrations at NDRO; H) Station difference profiles of 2019-11-7.

3.3 Kinetic Controls on Methanotrophic Bacterial Community

In order to assess the efficacy of our approach to methane oxidation rate measurement in the SBB, we conducted 3 experiments (time course incubation experiment, oxygen concentration alteration experiment, and methane concentration alteration experiment) to determine how the metabolism of the methanotrophic microbial community varied with respect to duration of incubation and supplementation of substrates – methane and oxygen. Due to limited sample volume available per sampling, each experiment was performed during a different sampling expedition.

Results from time course incubations (samples from Connell-092419), including sample sets for six different depths each collected at three different times, indicate a linear consumption of substrate over time for each sample set – between 1 and 3 days of incubation (Fig 5A). In turn, these results indicate a constant rate of metabolism by the methanotrophic community over this period of time, for each sample set. The implication of this observation is that the metabolic rate of the methanotrophic community tends to be consistent for a given set of conditions in the incubations, as has been observed in other systems (Bussmann et al., 2015).

Results from the oxygen concentration alteration experiment (samples from Connell-100419) are displayed in Fig 5B, which was designed to assess the effect of oxygen on the rate of methane consumption for the low-oxygen waters of the SBB. In this case, sample sets from six different depths were amended with oxygen to achieve three different oxygen concentrations. The results show no appreciable impact of oxygen concentration on the rate of consumption, even for the samples collected at depths with ambient oxygen of <5 μM.

Unlike oxygen, methane concentration (samples from Connell-102119) exhibited a linear relationship with oxidation rate for all six sample sets investigated (Fig 5C). Such a linear relationship has been observed previously (Mau et al., 2013; Bussmann et al., 2015) and is consistent with the kinetic relationship used to derive in-situ rates (Eq 3).

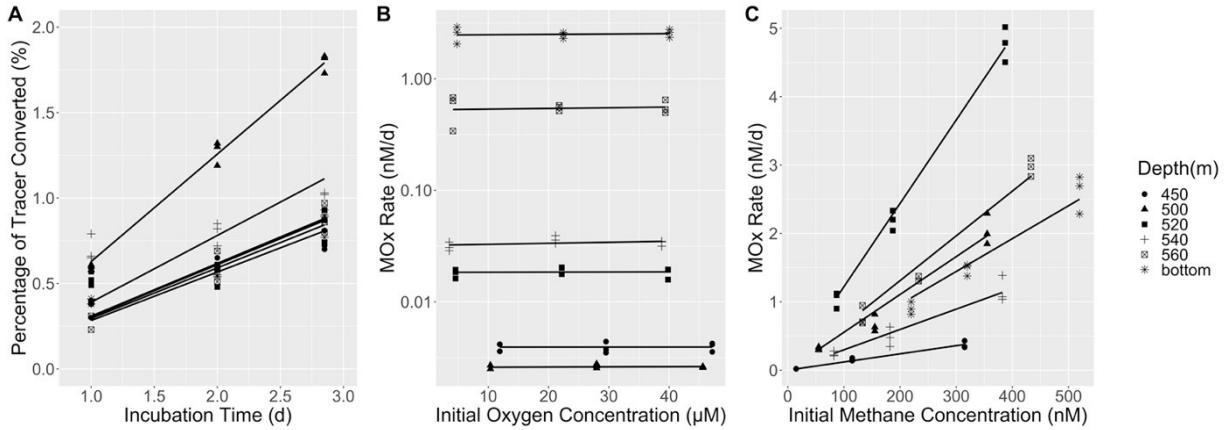

Figure 5. A) Percentage of ^{3}H-CH_4 tracer that was converted to ^{3}H-H_2O during the time-course incubation. Adjusted R^2 values of the linear regressions range from 0.937 - 0.999. B) Influence of the initial oxygen concentration on the resulting MOx rates. Note that the y-axis is on a logarithmic scale. Linear regressions generated for each sampling depth indicate no statistical support for a non-zero slope. C) Influence of the initial methane concentration on the resulting MOx rates. Adjusted R^2 values of the linear regressions range from 0.971 - 0.997. Symbols denote samples from different depths.

4. Discussion

4.1 Driving Forces of Methane Concentration and MOx Rate Changes

A comparison of time series changes in oxygen concentration, nitrate concentration, methane concentration and MOx rate (Fig 3) provides new insight as to how these parameters change over a seasonal deoxygenation and reoxygenation event. From Figure 3 a sequential behavior is apparent in the deep water column, with a decline in oxygen concentration leading the decline of nitrate concentration. Methane accumulation preceded a pronounced decline of oxygen and nitrate. Changes to MOx rate, which reflects the activity of the methanotroph community, followed methane concentration change, with a short lag in time.

Previous studies have demonstrated that anoxic and hypoxic conditions can cause the buildup of methane in the water column (Fanning and Pilson, 1972; Reeburgh, 1976; Reeburgh et al., 1991; Pack et al., 2015). We attribute the seasonal buildup of methane in the deep water column of SBB to the seasonal water column oxygen deprivation. Several factors may contribute to the accumulation of methane. First, seasonal deoxygenation of deep SBB water column usually happens after spring, when primary producers thrive utilizing the upwelled nutrients (Bograd et al., 2002; Goericke et al., 2015). The increased productivity in the surface supplies the sediment with more organic materials, which may lead to enhanced methanogenesis in shallow sediment layers or suspended particulate matter (Bange et al., 2010; Steinle et al., 2017). Second, the establishment of seasonal deoxygenation in the deep SBB water column after spring coincides with the development of water column stratification, which hinders vertical mixing of water (Steinle et al., 2017). Stratification has been shown to facilitate the accumulation of methane (Naqvi et al., 2010). Third, reduced water column oxygen concentration is expected to reduce the flux of oxygen available to sediment-hosted methanotrophs. This could lead to an increased

methane flux from the sediments driven by substrate (oxygen) limitation or habitat reduction for methanotrophs. Importantly, we suggest that water column oxygen deprivation has an indirect (rather than any direct) controlling effect on methane concentration, potentially modulating spatial distributions and activities of methanogenic and or methanotrophic communities and processes.

We attribute the rapid loss of methane in the water column in November 2019 to the highly active methanotroph community that started to develop and grow prior to November, rather than the additional oxygen that appeared in the basin at this time. It is indicated by our oxygen concentration alteration experiment that – even at low oxygen concentration – oxygen is not rate limiting for methanotrophy in the SBB. This implies that additional oxygen would not have a significant influence on MOx rate for the deep SBB methanotroph community. We therefore inferred that the introduced oxygen would have exerted little direct effect on the methane oxidation rate, and further, the methane loss would not be caused by the additional oxygen. Similar results have been observed by Steinle et al. 2017; in their study, MOx rates were the highest for samples with sub-micromolar oxygen concentrations, and increased oxygen concentrations either resulted in little change or decreased MOx rates. Notably, their samples originated from shallow coastal marine environments.

The methanotroph community increased in activity from June through October of 2019 (summer to fall 2019). The establishment of the methanotroph community is mainly controlled by the availability of methane in the surrounding environment. As shown by our substrate alteration experiments, oxygen concentration is not the direct limiting factor for methanotroph activity across the range tested (3.6 - 47.1 μM), and presumably the same is true for cellular growth. Methane

availability, itself modulated by oxygen deprivation, appeared to be the primary factor controlling the establishment of the methanotroph community.

The methanotroph community sustained the elevated activity into February and March of 2020 (late winter and early spring 2020), despite the decline in ambient methane concentrations. The reason methanotrophic activity is sustained in the absence of elevated methane concentrations is unclear. One possible explanation is that even though the methane concentration was low, methane supply (e.g., from sediments) was sufficient to support a more active methanotroph community. Another possible explanation is that the pulse of methane observed in October and November of 2019 might have acted as a "priming" mechanism for the methanotroph community – growing the population size and creating a methane demand that persisted even after the methane was mostly consumed. Finally, low oxygen concentration in the water could also reduce the grazing pressure on methanotrophic bacteria, allowing the community to persist for months in the deep water despite an insufficient methane supply (Devlin et al., 2015; Steinle et al., 2017). Whatever the mechanism, the transient methane pulse that accompanied the observed oxygen loss in the Santa Barbara Basin triggered the development of a methanotrophic community that persisted beyond the period when methane was elevated. This microbial memory effect is a similar phenomenon observed in the Gulf of Mexico following the transient methane release from Deepwater Horizon (Kessler et al., 2011; Valentine et al., 2012; Crespo-Medina et al., 2014).

4.2 Evidence for an Intrusion Event Over the Western Sill

Evidence for an intrusion event over the western sill is apparent in the comparison of oxygen concentration and density, for stations SDRO and NDRO, on 2019-10-30 and 2019-11-7 (Fig 6).

These plots reveal similar distributions between the two stations on 2019-10-30 giving way to more highly oxygenated waters on 2019-11-7, for both stations. Greater oxygen concentrations on 2019-11-7 indicate a substantial intrusion event, with variability between locations indicating depth dependence for processes that drive the pattern of lateral mixing.

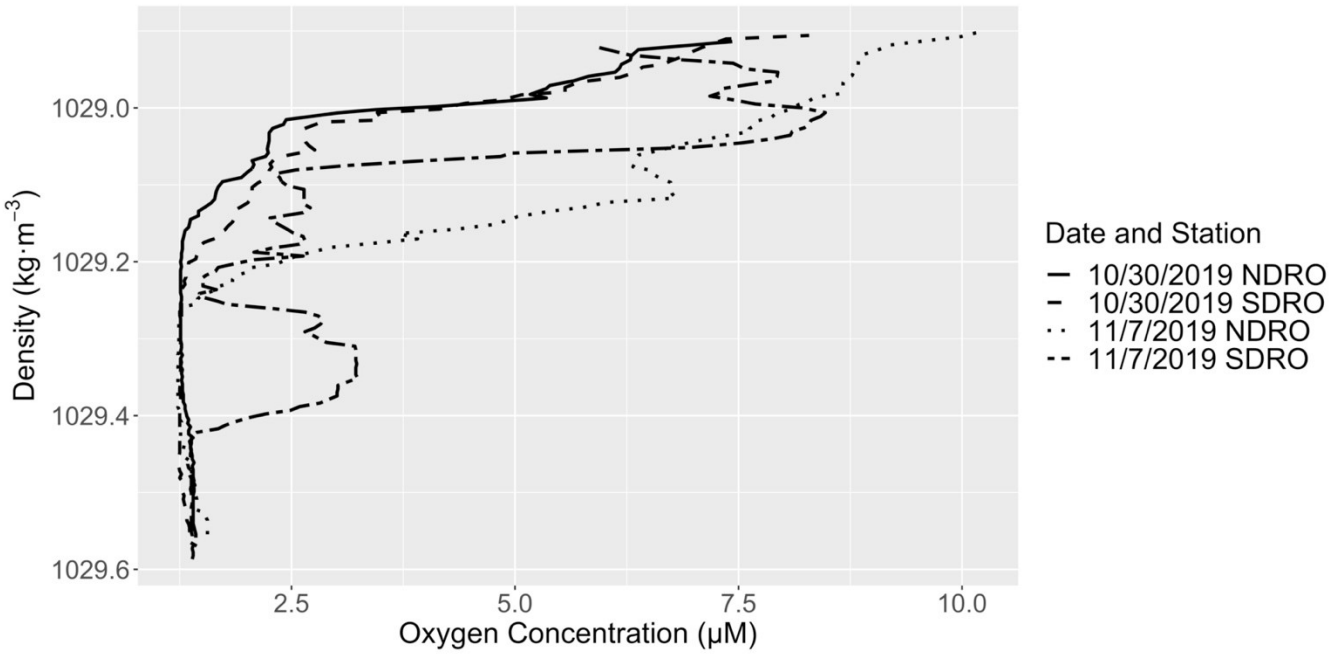

Figure 6. Profiles of density versus oxygen concentration for the SBB deep water column (450 m-bottom). Four profiles are shown and provide additional evidence for an intrusion event from the western sill between 2019-10-30 and 2019-11-7.

Evidence for an intrusion event over the western sill is also shown by Fig 4. The increased oxygen concentrations of both stations on 2019-11-7 are consistent with an intrusion of water over the western sill into the deep SBB. The resulting vertical distributions of water masses indicate vertical stratification consistent with isopycnal lenses, blobs or fingers of intruding water spilling over the western sill.

The oxygen inversions observed on 2019-11-7 are similar in form to SBB oxygen profiles sometimes captured by CALCOFI (Fig 1) and provide useful context in interpreting those data.

Specifically, oxygen variability may sometimes represent transient mixing processes along isopycnals that effectively provides a small pulse of oxygen into the deep SBB but does not represent a complete flushing event for which deep water is replaced by cascading waters of higher density.

With the above analysis, we have evidence for the occurrence of an intrusion event over the western sill. However, the substantial decline of integrated methane burden (Fig 4) in the deep SBB from 2019-10-30 to 2019-11-7 at both NDRO and SDRO is difficult to be explained by this intrusion event, in the absence of a large-scale flushing event. Instead, the available data are consistent with a pulse of methanotrophic activity peaking around this time, after experiencing an exponential increase in September and October (Fig 3D). The observed exponential growth in methanotrophic activity clearly preceded the intrusion event captured on 2019-11-7. Based on our observations, it is indicated that an interplay of oxygen, mixing, and bacterial population dynamics exerted non-steady-state control on the accumulation and loss of methane in the deep SBB.

5. Conclusions

This study demonstrates that seasonal deoxygenation events can lead to the buildup of deep water column methane concentrations, and in turn prompt the activity of the methanotroph community. The response of the methanotroph community leads to the removal of methane from the deep water column. We also show that MOx rate is dependent on methane but not oxygen concentration even at very low ambient oxygen concentration (the lowest oxygen tested was 3.6 μM). While other factors may structure microbial response to methane in other environments, our results provide a useful case study to understand the time scale and controls that act on the development of a marine

methanotrophic community when faced with gradual deoxygenation and episodic rejuvenation. The deep water column of SBB provides a useful example of methane dynamics driven by seasonal oxygen changes. The results provide insights for the understanding of temporal dynamics and environmental controls on the efficiency of the methanotrophic biofilter in the deep water column. Not only can insights from this work be used to understand methane dynamics in other marine basins, but these results also inform our understanding for how methane dynamics may change in the face of global expansion of oxygen minimum zones.

Declaration of Competing Interest

The authors declare that they have no known competing financial interests or personal relationships that could have appeared to influence the work reported in this paper.

Acknowledgements

We thank: the *R/V Atlantis* Captain, Crew, and Science Party of Research Cruise AT42-19; Christian Orsini and Christoph Pierre for captaining sample expeditions; UCSB MSI Analytical Lab for analyzing nitrate concentrations; Dr. Craig Carlson's lab for assistance with oxygen concentration measurements; Dr. Alyson Santoro for providing oxygen concentration for December, 2019; Xiadani Moreno for assisting with methane concentration measurements; Dr. Burch Fischer for providing the SBB bathymetry map; as well as UCSB and UCLA radiation safety offices for transporting the $^{3}H\text{-}CH_4$ tracer. Funding for this work was provided by the US National Science Foundation, NSF OCE-1756947 and OCE-1830033 (to DLV) and OCE-1829981 (to TT).

Research Data

Research Data associated with this article can be accessed at the Biological & Chemical Oceanography Data Management Office, DOIs: https://doi.org/10.26008/1912/bco-dmo.872703.1; https://doi.org/10.26008/1912/bco-dmo.872687.1; https://doi.org/10.26008/1912/bco-dmo.872665.1; https://doi.org/10.26008/1912/bco-dmo.872652.1.

References

de Angelis M. A., Lilley M. D., Olson E. J. and Baross J. A. (1993) Methane oxidation in deep-sea hydrothermal plumes of the endeavour segment of the Juan de Fuca Ridge. *Deep Sea Research Part I: Oceanographic Research Papers* **40**, 1169–1186.

Bange H. W., Bergmann K., Hansen H. P., Kock A., Koppe R., Malien F. and Ostrau C. (2010) Dissolved methane during hypoxic events at the Boknis Eck time series station (Eckernforde Bay, SW Baltic Sea). *Biogeosciences* **7**, 1279–1284.

Bograd S. J., Schwing F. B., Castro C. G. and Timothy D. A. (2002) Bottom water renewal in the Santa Barbara Basin. *J. Geophys. Res.* **107**, 9-1-9–9.

Bussmann I., Matousu A., Osudar R. and Mau S. (2015) Assessment of the radio 3H-CH4 tracer technique to measure aerobic methane oxidation in the water column. *Limnology and Oceanography: Methods* **13**, 312–327.

Crespo-Medina M., Meile C. D., Hunter K. S., Diercks A.-R., Asper V. L., Orphan V. J., Tavormina P. L., Nigro L. M., Battles J. J., Chanton J. P., Shiller A. M., Joung D.-J., Amon R. M. W., Bracco A., Montoya J. P., Villareal T. A., Wood A. M. and Joye S. B. (2014) The rise and fall of methanotrophy following a deepwater oil-well blowout. *Nature Geosci* **7**, 423–427.

Devlin S. P., Saarenheimo J., Syväranta J. and Jones R. I. (2015) Top consumer abundance influences lake methane efflux. *Nat Commun* **6**, 8787.

Ding H. and Valentine D. L. (2008) Methanotrophic bacteria occupy benthic microbial mats in shallow marine hydrocarbon seeps, Coal Oil Point, California. *Journal of Geophysical Research: Biogeosciences* **113**.

Du M., Yvon-Lewis S., Garcia-Tigreros F., Valentine D. L., Mendes S. D. and Kessler J. D. (2014) High Resolution Measurements of Methane and Carbon Dioxide in Surface

Waters over a Natural Seep Reveal Dynamics of Dissolved Phase Air–Sea Flux. *Environ. Sci. Technol.* **48**, 10165–10173.

Fanning K. A. and Pilson M. E. Q. (1972) A model for the anoxic zone of the Cariaco Trench. *Deep Sea Research and Oceanographic Abstracts* **19**, 847–863.

Goericke R., Bograd S. J. and Grundle D. S. (2015) Denitrification and flushing of the Santa Barbara Basin bottom waters. *Deep Sea Research Part II: Topical Studies in Oceanography* **112**, 53–60.

Griffiths R. P., Caldwell B. A., Cline J. D., Broich W. A. and Morita R. Y. (1982) Field Observations of Methane Concentrations and Oxidation Rates in the Southeastern Bering Sea. *Appl Environ Microbiol* **44**, 435–446.

Gründger F., Probandt D., Knittel K., Carrier V., Kalenitchenko D., Silyakova A., Serov P., Ferré B., Svenning M. M. and Niemann H. (2021) Seasonal shifts of microbial methane oxidation in Arctic shelf waters above gas seeps. *Limnology and Oceanography* **66**, 1896–1914.

Heintz M. B., Mau S. and Valentine D. L. (2012) Physical control on methanotrophic potential in waters of the Santa Monica Basin, Southern California. *Limnology and Oceanography* **57**, 420–432.

Hill T. M., Kennett J. P. and Spero H. J. (2003) Foraminifera as indicators of methane-rich environments: A study of modern methane seeps in Santa Barbara Channel, California. *Marine Micropaleontology* **49**, 123–138.

Hinrichs K.-U., Hayes J. M., Sylva S. P., Brewer P. G. and DeLong E. F. (1999) Methane-consuming archaebacteria in marine sediments. *Nature* **398**, 802–805.

Hinrichs K.-U., Hmelo L. R. and Sylva S. P. (2003) Molecular Fossil Record of Elevated Methane Levels in Late Pleistocene Coastal Waters. *Science* **299**, 1214–1217.

Hornafius J. S., Quigley D. and Luyendyk B. P. (1999) The world's most spectacular marine hydrocarbon seeps (Coal Oil Point, Santa Barbara Channel, California): Quantification of emissions. *J. Geophys. Res.* **104**, 20703–20711.

Joung D., Leonte M., Valentine D. L., Sparrow K. J., Weber T. and Kessler J. D. (2020) Radiocarbon in Marine Methane Reveals Patchy Impact of Seeps on Surface Waters. *Geophysical Research Letters* **47**, e2020GL089516.

Kessler J. D., Valentine D. L., Redmond M. C., Du M., Chan E. W., Mendes S. D., Quiroz E. W., Villanueva C. J., Shusta S. S., Werra L. M., Yvon-Lewis S. A. and Weber T. C. (2011) A Persistent Oxygen Anomaly Reveals the Fate of Spilled Methane in the Deep Gulf of Mexico. *Science* **331**, 312–315.

Kinnaman F. S., Valentine D. L. and Tyler S. C. (2007) Carbon and hydrogen isotope fractionation associated with the aerobic microbial oxidation of methane, ethane, propane and butane. *Geochimica et Cosmochimica Acta* **71**, 271–283.

Knittel K. and Boetius A. (2009) Anaerobic Oxidation of Methane: Progress with an Unknown Process. *Annual Review of Microbiology* **63**, 311–334.

Kosiur D. R. and Warford A. L. (1979) Methane production and oxidation in Santa Barbara Basin sediments. *Estuarine and Coastal Marine Science* **8**, 379–385.

Li C., Sessions A. L., Kinnaman F. S. and Valentine D. L. (2009) Hydrogen-isotopic variability in lipids from Santa Barbara Basin sediments. *Geochimica et Cosmochimica Acta* **73**, 4803–4823.

Mau S., Blees J., Helmke E., Niemann H. and Damm E. (2013) Vertical distribution of methane oxidation and methanotrophic response to elevated methane concentrations in stratified waters of the Arctic fjord Storfjorden (Svalbard, Norway). *Biogeosciences* **10**, 6267–6268.

Mau S., Heintz M. B., Kinnaman F. S. and Valentine D. L. (2010) Compositional variability and air-sea flux of ethane and propane in the plume of a large, marine seep field near Coal Oil Point, CA. *Geo-Marine Letters* **30**, 367–378.

Mau S., Heintz M. B. and Valentine D. L. (2012) Quantification of CH4 loss and transport in dissolved plumes of the Santa Barbara Channel, California. *Continental Shelf Research* **32**, 110–120.

Mau S., Valentine D. L., Clark J. F., Reed J., Camilli R. and Washburn L. (2007) Dissolved methane distributions and air-sea flux in the plume of a massive seep field, Coal Oil Point, California. *Geophys. Res. Lett.* **34**, L22603.

Middelburg J. J. and Levin L. A. (2009) Coastal hypoxia and sediment biogeochemistry. *Biogeosciences* **6**, 1273–1293.

Naqvi S. W. A., Bange H. W., Farias L., Monteiro P. M. S., Scranton M. I. and Zhang J. (2010) Marine hypoxia/anoxia as a source of CH4 and N2O. *Biogeosciences* **7**, 2159–2190.

Pack M. A., Heintz M. B., Reeburgh W. S., Trumbore S. E., Valentine D. L., Xu X. and Druffel E. R. M. (2011) A method for measuring methane oxidation rates using low-levels of 14C-labeled methane and accelerator mass spectrometry. *Limnology and Oceanography: Methods* **9**, 245–260.

Pack M. A., Heintz M. B., Reeburgh W. S., Trumbore S. E., Valentine D. L., Xu X. and Druffel E. R. M. (2015) Methane oxidation in the eastern tropical North Pacific Ocean water column. *Journal of Geophysical Research: Biogeosciences* **120**, 1078–1092.

Padilla A. M., Loranger S., Kinnaman F. S., Valentine D. L. and Weber T. C. (2019) Modern Assessment of Natural Hydrocarbon Gas Flux at the Coal Oil Point Seep Field, Santa Barbara, California. *Journal of Geophysical Research: Oceans* **124**, 2472–2484.

Reay D. S., Smith P., Christensen T. R., James R. H. and Clark H. (2018) Methane and Global Environmental Change. *Annual Review of Environment and Resources* **43**, 165–192.

Reeburgh W. S. (1976) Methane consumption in Cariaco Trench waters and sediments. *Earth and Planetary Science Letters* **28**, 337–344.

Reeburgh W. S. (2007) Oceanic Methane Biogeochemistry. *Chem. Rev.* **107**, 486–513.

Reeburgh W. S., Ward B. B., Whalen S. C., Sandbeck K. A., Kilpatrick K. A. and Kerkhof L. J. (1991) Black Sea methane geochemistry. *Deep-Sea Research, Part A* **38**, S1189–S1210.

Reimers C. E., Lange C. B., Tabak M. and Bernhard J. M. (1990) Seasonal spillover and varve formation in the Santa Barbara Basin, California. *Limnology and Oceanography* **35**, 1577–1585.

Segarra Guerrero R., Gomezbenito C. and Martinez Calatayud J. (1996) Flow-injection analysis-spectrophotometric determination of nitrite and nitrate in water samples by reaction with proflavin. *Talanta* **43**, 239–246.

Sholkovitz E. (1973) Interstitial water chemistry of the Santa Barbara Basin sediments. *Geochimica et Cosmochimica Acta* **37**, 2043–2073.

Sholkovitz E. R. and Gieskes J. M. (1971) A physical-chemical study of the flushing of the Santa Barbara Basin. *Limnology and Oceanography* **16**, 479–489.

Sholkovitz E. and Soutar A. (1975) Changes in the composition of the bottom water of the Santa Barbara Basin: effect of turbidity currents. *Deep Sea Research and Oceanographic Abstracts* **22**, 13–21.

Sigman D. M., Robinson R., Knapp A. N., van Geen A., McCorkle D. C., Brandes J. A. and Thunell R. C. (2003) Distinguishing between water column and sedimentary denitrification in the Santa Barbara Basin using the stable isotopes of nitrate. *Geochemistry, Geophysics, Geosystems* **4:5**.

Solomon S., Qin D., Manning M., Marquis M., Averyt K., Tignor M. M. B., Miller H. L. Jr. and Chen Z. eds. (2007) *Climate change 2007: The physical science basis*., Cambridge University Press, Cambridge; New York.

Steinle L., Graves C. A., Treude T., Ferré B., Biastoch A., Bussmann I., Berndt C., Krastel S., James R. H., Behrens E., Böning C. W., Greinert J., Sapart C.-J., Scheinert M., Sommer S., Lehmann M. F. and Niemann H. (2015) Water column methanotrophy controlled by a rapid oceanographic switch. *Nature Geosci* **8**, 378–382.

Steinle L., Maltby J., Treude T., Kock A., Bange H. W., Engbersen N., Zopfi J., Lehmann M. F. and Niemann H. (2017) Effects of low oxygen concentrations on aerobic methane oxidation in seasonally hypoxic coastal waters. *Biogeosciences* **14**, 1631–1645.

Steinle L., Schmidt M., Bryant L., Haeckel M., Linke P., Sommer S., Zopfi J., Lehmann M. F., Treude T. and Niemannn H. (2016) Linked sediment and water-column methanotrophy at a man-made gas blowout in the North Sea: Implications for methane budgeting in seasonally stratified shallow seas. *Limnology and Oceanography* **61**, S367–S386.

Strous M. and Jetten M. S. M. (2004) Anaerobic Oxidation of Methane and Ammonium. *Annual Review of Microbiology* **58**, 99–117.

Tavormina P. L., Ussler W., Joye S. B., Harrison B. K. and Orphan V. J. (2010) Distributions of putative aerobic methanotrophs in diverse pelagic marine environments. *ISME J* **4**, 700–710.

Torres-Beltrán M., Hawley A. K., Capelle D. W., Bhatia M. P., Durno E. W., Tortell P. D. and Hallam S. J. (2016) Methanotrophic community dynamics in a seasonally anoxic fjord: Saanich Inlet, British Columbia. *Front. Mar. Sci.* **3:268**.

Treude, T. (2004) Anaerobic oxidation of methane in marine sediments. Doctoral dissertation, Universität Bremen Bremen.

Valentine D. L., Blanton D. C., Reeburgh W. S. and Kastner M. (2001) Water column methane oxidation adjacent to an area of active hydrate dissociation, Eel River Basin. *Geochimica et Cosmochimica Acta* **65**, 2633–2640.

Valentine D. L., Mezic I., Macesic S., Crnjaric-Zic N., Ivic S., Hogan P. J., Fonoberov V. A. and Loire S. (2012) Dynamic autoinoculation and the microbial ecology of a deep water hydrocarbon irruption. *Proceedings of the National Academy of Sciences* **109**, 20286–20291.

Ward B. B. and Kilpatrick K. A. (1993) Methane oxidation associated with mid-depth methane maxima in the Southern California Bight. *Continental Shelf Research* **13**, 1111–1122.

Ward B. B., Kilpatrick K. A., Novelli P. C. and Scranton M. I. (1987) Methane oxidation and methane fluxes in the ocean surface layer and deep anoxic waters. *Letters to Nature* **327**, 226–229.

Ward B. B., Kilpatrick K. A., Wopat A. E., Minnich E. C. and Lidstrom M. E. (1989) Methane oxidation in Saanich inlet during summer stratification. *Continental Shelf Research* **9**, 65–75.

Warford A. L., Kosiur D. R. and Doose P. R. (1979) Methane production in Santa Barbara basin sediments. *Geomicrobiology Journal* **1**, 117–137.

Weiss R. F. (1970) The solubility of nitrogen, oxygen and argon in water and seawater. *Deep Sea Research and Oceanographic Abstracts* **17**, 721–735.

Zhang X., Hester K. C., Ussler W., Walz P. M., Peltzer E. T. and Brewer P. G. (2011) In situ Raman-based measurements of high dissolved methane concentrations in hydrate-rich ocean sediments. *Geophysical Research Letters* **38**, L08605.